


Direct Path from Turbulence to Time-Periodic Solutions

Chaitanya S. Paranjape^{1,*}, Gökhan Yalmaz^{1,*}, Johann Duguet², Nazmi Burak Budanur^{1,3} and Björn Hof^{1,†}

¹*Institute of Science and Technology Austria (ISTA), 3400 Klosterneuburg, Austria*

²*LISN-CNRS, Campus Universitaire d'Orsay, Université Paris-Saclay, 91405 Orsay, France*

³*Max Planck Institute for the Physics of Complex Systems (MPIPKS), 01187 Dresden, Germany*

 (Received 7 August 2022; revised 2 May 2023; accepted 7 June 2023; published 21 July 2023)

Viscous flows through pipes and channels are steady and ordered until, with increasing velocity, the laminar motion catastrophically breaks down and gives way to turbulence. How this apparently discontinuous change from low- to high-dimensional motion can be rationalized within the framework of the Navier-Stokes equations is not well understood. Exploiting geometrical properties of transitional channel flow we trace turbulence to far lower Reynolds numbers (Re) than previously possible and identify the complete path that reversibly links fully turbulent motion to an invariant solution. This precursor of turbulence destabilizes rapidly with Re , and the accompanying explosive increase in attractor dimension effectively marks the transition between deterministic and *de facto* stochastic dynamics.

DOI: [10.1103/PhysRevLett.131.034002](https://doi.org/10.1103/PhysRevLett.131.034002)

The origin of turbulence in pipe and channel flows has been debated for over a century. In recent years much effort has been dedicated to link the formation of turbulence to simple invariant solutions of the governing Navier-Stokes equations (periodic orbits, equilibria, and traveling waves), which are commonly referred to as exact coherent structures (ECS) [1,2]. ECSs are suggested as building blocks of the turbulent dynamics [3–7]. However, efforts to directly link specific ECSs to the turbulent state, let alone to identify a reversible path connecting the two, have remained so far unsuccessful. While specific ECSs have been identified as starting points of bifurcation sequences into chaos [8–12], the traceable path in parameter space towards turbulence in all these cases ends at a *boundary crisis* [13]. At this point the attractor ceases to exist, giving way to short-lived transient chaos. Although a sufficiently fast ramp up in Re will prevent relaminarization and lead to turbulence, strictly, this only shows that the chosen route leads to the basin of attraction of turbulence [14]. It does not necessarily prove, however, that the turbulent state originates from the specific ECSs, e.g., via a sequence of bifurcations. An unambiguous way to determine its roots would require starting directly from the turbulent state and tracing it quasistatically down to its origin, a path prohibited by the aforementioned relaminarization barrier.

This situation is markedly different from simpler transition scenarios encountered, e.g., in supercritical Taylor-Couette flow and Rayleigh-Bénard convection. In such cases a linear instability of the base flow gives rise to a *primary vortex state*, which is the starting point of the bifurcation sequence leading to chaotic and eventually high-dimensional, turbulent motion. In particular, signatures of the primary vortex state tend to persist and can be detected in turbulent flow fields at values of Re several

orders of magnitude larger than the instability threshold [15]. Hence, the role of the primary state and the connection with the subsequent dynamics is without question.

The purpose of the present study is to unambiguously identify the equivalent of the primary vortex state in aforementioned linearly stable flows, i.e., to determine the precursor turbulence originates from for channel flow. While given the transient nature of turbulence this may appear unfeasible, we show that by bypassing the regime of fully localized turbulent structures, turbulence can be traced beyond the transient regime all the way to its origin. The reverse path towards fully turbulent flow extends across a considerable Re range. However, surprisingly, stochasticity arises directly at the outset of this route, when the dimension increases explosively across a minute variation in parameter.

Turbulence is space filling at sufficiently large Re (Re is based here on the half-gap h , the kinematic viscosity and the laminar centerline velocity). At lower velocities turbulence becomes spatiotemporally intermittent (STI) and tends to organize in stripes interspersed with laminar regions [16–19]. Below $Re \approx 650$ [20] stripes are short lived. Under standard circumstances this transient nature prevents continuation of turbulence towards lower Re (see Fig. 1 top row) and prohibits further insights into its dynamical origin.

In an attempt to circumvent this problem, we carry out direct numerical simulations in a domain that, on the one hand, is sufficiently large to capture generic turbulence at high Re and, on the other hand, is of the minimal size to capture turbulent stripes of a prescribed angle. Such minimal flow units for stripes [21] make use of the freedom to choose the orientation of the computational domain in the periodic directions. In our case we selected a tilt angle

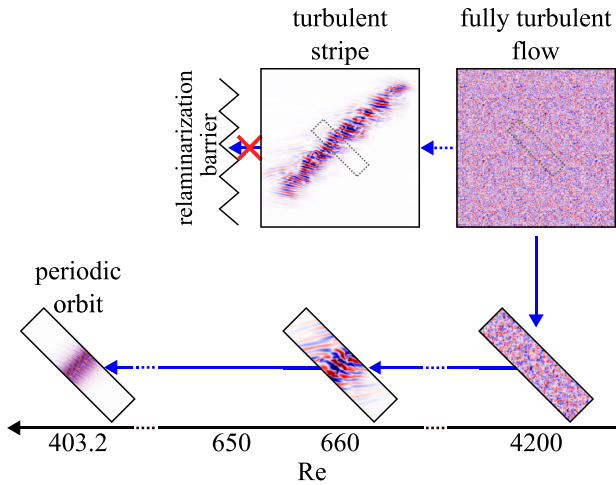


FIG. 1. Sketch of the Re descent in a tilted domain vs large nontilted domains. Shown are wall-normal velocity (v) contours (range limited from $v = -0.1$ in blue to $v = 0.1$ in red) in the midplane for various values of Re . Flow is from left to right. Dashed rectangles indicate the size and orientation of the tilted domain. (Bottom row images) 10×40 sized tilted domain investigated in this work. (Top row images) 100×100 crops from nontilted domains (display scale is half that of bottom row images).

of 45° with respect to the streamwise direction. Owing to the periodic boundary conditions stripes align at this prescribed angle (see Fig. 1 bottom row for examples). This choice of a 45° angle is motivated by channel experiments where the same orientation is observed for stripes close to the onset of turbulence [17]. The selected domain size, as in [22], is 10×40 ($L_x \times L_z$) in units of h . The incompressible Navier-Stokes equations are advanced in time using a standard spectral method in a three-dimensional domain with periodic boundary conditions in the plane and no-slip at the walls, with constant mass flux [23–25].

The simulations started from a fully turbulent flow field at $Re = 4200$ (corresponding to a friction Reynolds number of $Re_\tau = 180$ [26]). Re was subsequently reduced in several steps down to $Re_{STI}^{full} \approx 1500$, where turbulence becomes patterned [27] (see Table I for a list of transitions encountered for decreasing Re). From here the descent was continued in small steps, allowing the flow to settle for 500 advective time units (ratio of h by the laminar centerline velocity) between consecutive steps. Below $Re = 900$ the step size was set to $\Delta Re = 2$. Typical adjustments of the turbulent flow occur within less than 100 advective time units. Once Re falls below $Re_{trans}^{STI} \approx 650$, and in agreement with the aforementioned experimental observations [20] stripes are found to decay. However, in the present case lifetimes remain much larger and typically exceed several thousand advective time units. In agreement with these recent experiments we hence propose that $Re_{trans}^{STI} \approx 650$ is close to the point above which turbulence in extended

TABLE I. List of Reynolds numbers, at which the dynamics changes qualitatively. The third column specifies the dynamics observed below the given Re in simulations in the 10×40 sized tilted domain. Subscripts refer to the observations below the given Re whereas superscripts refer to the observations above.

Name	Value	Observations below Re
Re_{STI}^{full}	≈ 1500	Spatio-temporal intermittency
Re_{trans}^{STI}	≈ 650	Transient chaos
Re_{chaos}^{trans}	≈ 420	Sustained chaos
Re_{chaos}^{torus}	412.8	Quasiperiodicity
Re_{PO}^{torus}	403.2	Periodic orbits ^a

^aSee SM [27] for a table continued beyond this point.

domains (large L_z) first becomes sustained. In our tilted domain simulations lifetimes below this threshold remain sufficiently long for turbulence to reach what can be considered a statistically quasisteady state.

As shown in the Supplemental Material, movie [27], the thereby stabilized stripe is followed far below Re_{trans}^{STI} , a regime previously inaccessible in experiments and simulations. With decreasing Re the perturbation kinetic energy of the stripe reduces [see Fig. 2(a)], nevertheless fluctuations remain large and the flow is strongly chaotic even for Re as low as 450. For lower Re , as attested by the phase portrait of the dynamics in Fig. 2(b), fluctuations reduce fast in amplitude and the state space region explored by the chaotic dynamics shrinks substantially. Eventually, the dynamics ceases to be chaotic (Re_{torus}^{chaos}) and instead becomes quasiperiodic: the trajectory evolves on a 2-torus in state space [Fig. 2(c)], and below Re_{PO}^{torus} becomes periodic [see Fig. 2(d) and the Supplemental Material, movie [27]]. The previously turbulent stripe hence simplifies to an exact coherent structure (Fig. 1). Despite its dynamical simplicity, the key spatial features, such as streamwise localization, characteristic spacing of streaks and vortices, associated large-scale flow parallel to the interface [28], have been preserved all along this reduction in Re . As we further discuss in the Supplemental Material [27], the periodic orbit (PO) can be continued [25,29] to even lower Re . It is shown to originate from a lower branch traveling wave, an edge state previously identified in [17,30]. To probe the robustness of this transition scenario, we repeated the descent in a much larger (10×120) domain and observed the same bifurcation sequence. A notable aspect of the above Re reduction is the sudden decrease of the attractor size at the final stages of the approach to the PO: the energy fluctuations displayed by the turbulent stripe at $Re = 450$ [Fig. 2(b)] are more than 2 orders of magnitude larger than those of the PO at $Re = 402$ [Fig. 2(d)].

To obtain a better understanding of the emergence of turbulence, we take the PO as the starting point and investigate how the dynamics unfolds in the reverse

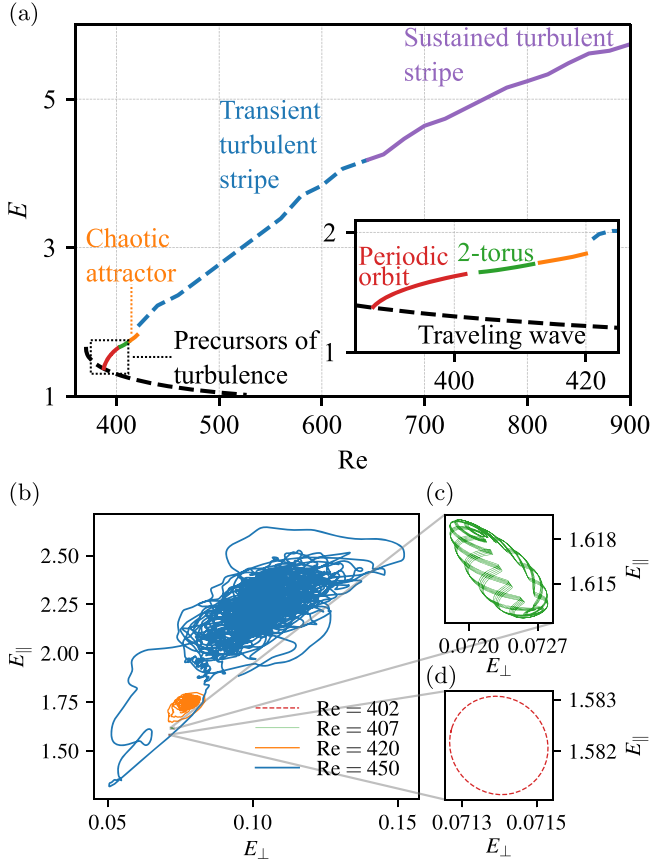


FIG. 2. Stripe turbulence during the Re descent. (a) Time-averaged perturbation kinetic energy E vs Re . Annotations refer to the respective dynamics encountered as Re is decreased. (b) $(E_{\perp}, E_{\parallel})$ phase portraits of the instantaneous dynamics at various Re demonstrating some of the dynamics annotated in (a), with enlarged panels for (c) the torus at $Re = 407$ and (d) the periodic orbit at $Re = 402$. E_{\perp} is the kinetic energy associated with the wall-normal component (v) of perturbation velocity \mathbf{u} , $E_{\perp} = \int_V v^2/2 dV$, and E the perturbation kinetic energy, $E = \int_V \mathbf{u} \cdot \mathbf{u}/2 dV$, where V is the computational domain. $E_{\parallel} = E - E_{\perp}$ is the kinetic energy associated with the in-plane components of perturbation velocity.

direction, i.e., with increasing Re . To this end we analyze the time series of the perturbation kinetic energy E . The method assumes the knowledge of consecutive values E_0, E_1, \dots, E_{n-1} , sampled every Δt . We first monitor the Hurst exponent $H(Re)$ associated with this time series of length n . H quantifies the correlation of a signal, and is defined as the exponent in the scaling relation

$$\mathbb{E}(R/S) \sim n^H, \quad n \rightarrow \infty, \quad (1)$$

where R is the range of the first n cumulative deviations from the mean, S the sum of the first n standard deviations, and \mathbb{E} stands for the expected value [31]. The quantity $D = 2 - H$ is interpreted as a fractal dimension, namely, that of the related signal [32]. As shown in Fig. 3, the stochastic

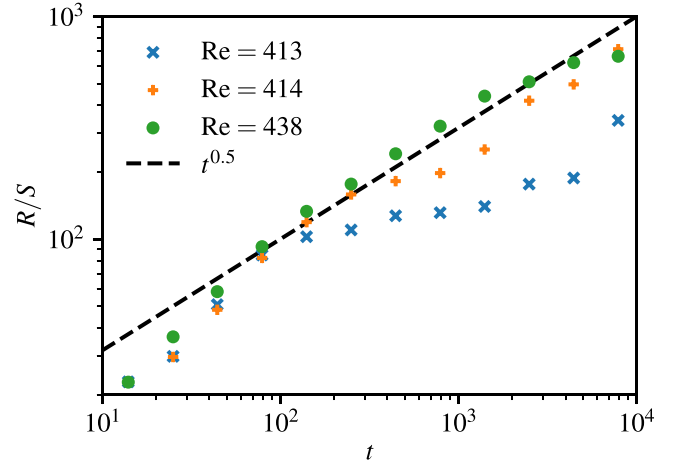


FIG. 3. R/S vs time in log-log scale, the slope of which defines the Hurst exponent (H). For $Re = 438$, a slope of $1/2$ is approached after 100 advective time units. $H = 1/2$ is expected for stochastic time series.

limit of $H = 1/2$ is already observed for a time horizon of 100 advective units at $Re = 438$, i.e., in the transient regime far below the onset of sustained turbulence [20]. This testifies that, for time horizons larger than 100 advective time units, the time series is indistinguishable from a purely stochastic signal. $O(100)$ advective time units match the typical time for localized turbulent structures to lose their memory after being created from a disturbance [33] (this timescale is also referred to as t_0 in lifetimes studies [34]).

As a further estimation of the trend towards stochasticity, we compute another fractal dimension, the correlation dimension D_2 of the full turbulent set, using the Grassberger-Procaccia algorithm [35,36]. For any integer $m > 0$ and any real $\varepsilon > 0$, $C_m(\varepsilon)$ is defined by

$$C_m(\varepsilon) = \lim_{n \rightarrow \infty} \frac{1}{n^2} \sum_{(j,k)}^n \Theta(\varepsilon - \|s_j - s_k\|_m), \quad (2)$$

where $s_k = (E_{k-(m-1)\tau}, \dots, E_{k-\tau}, E_k)$ is a delay vector in the m -dimensional embedded space, $\|\cdot\|_m$ a norm in that space, and Θ the Heaviside function. $\tau > 0$ is a finite time delay expressed in Eq. (2) in units of the sampling time Δt (in practice $\tau = 60$ advective time units, close to the correlation time). C_m counts temporal near recurrences in the m -dimensional embedded space. The dimension D_2 is fitted as the exponent, for large m , in the scaling relation

$$C_m(\varepsilon) \sim \varepsilon^{D_2}, \quad \varepsilon \rightarrow 0. \quad (3)$$

The amount of uncorrelated data necessary for the estimation of D_2 rises exponentially with its value [37], which in practice limits computations to values below 10. D_2 is computed here starting from the PO at $Re = 395$ up to

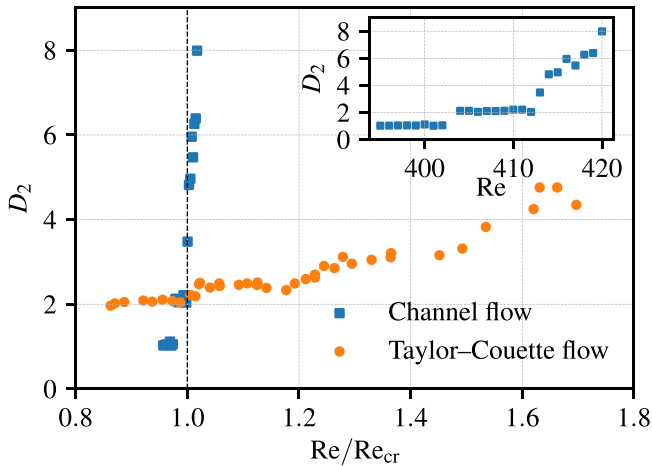


FIG. 4. Dimension (D_2) increase with Re at the onset of chaos in channel flow and Taylor-Couette flow. Blue squares are computed from time series of plane channel flow. Orange circles are from the turbulent Taylor-Couette flow experiments in Ref. [38]. Re_{cr} denotes the onset of chaos.

$Re_{chaos}^{trans} = 420$ deeper into the chaotic regime (blue squares in Fig. 4).

Figure 4 shows D_2 as a function of Re/Re_{cr} , where Re_{cr} stands for the onset of chaotic dynamics. For channel flow, Re_{cr} is identical to $Re_{torus}^{chaos} = 412.8$. Temporal chaos develops at a rapid pace: exceeding Re_{cr} by just over 1% causes the dimension to quadruple. This rapid increase is consistent with the high dimension estimated for turbulent channel flows for larger Re [39]. For comparison we show the classical case of the supercritical transition in Taylor-Couette flow [38] (orange circles in Fig. 4) where even a 50% increase above Re_{cr} results in only a doubling of the dimension.

The explosive dimension increase encountered in channel flow sharply limits the forecasting horizon directly at the onset of chaos, and decorrelates the fast turbulent internal dynamics of stripes from slow processes such as their proliferation and decay [40–42]. Moreover, the Hurst exponent of $1/2$ marks such slow processes as stochastic random events, a key requirement for the statistical nature of the percolation phase transition [43–46] encountered at higher Re in many shear flows.

Hydrodynamic stability concepts developed more than a century ago allowed for the identification of the first bifurcation to a nontrivial vortex state [47], and with it the starting point for the supercritical route to turbulence in linearly unstable flows. Finding corresponding flow states for the much more volatile transition characteristic of most flows of practical relevance, such as pipe and channel flows, has proven far more difficult. Exploiting that the statistics of turbulence are generic and independent of the numerical domain at sufficiently high Re (see Supplemental Material [27]), we selected a domain that stabilizes stripes in the transitional regime of channel flow. The stripe solutions identified in this configuration are

spatially periodic in the stripe direction and hence differ from the doubly localized stripes observed in experiments close to the critical point. It is likely that doubly localized stripe solutions [48,49] bifurcate from the ECS presented in this study. However, the continuous route from turbulence to ECSs identified here can only be established by bypassing the doubly localized stripe regime, in which flows unavoidably relaminarize (as illustrated in Fig. 1). Although the tilted domain may appear specific, the two states shown to be dynamically connected, i.e., the periodic orbit and fully turbulent flow, are generic to the classic channel flow problem and entirely independent of this particular choice.

A striking feature of the route towards turbulence is the abruptness of the dimension change directly at the onset of chaos, long before turbulence is observable in experiments. This steep dimension increase marks the border up to which deterministic concepts are suitable whereas above statistical mechanics descriptions become more appropriate, setting the stage for the nonequilibrium phase transition [40,43] encountered at larger Re .

We thank Baofang Song as well as the developers of Channelflow for sharing their numerical codes, and Mukund Vasudevan and Holger Kantz for fruitful discussions. This work was supported by a grant from the Simons Foundation (662960, B. H.).

*C. P. and G. Y. contributed equally to this work.

†bhof@ist.ac.at

- [1] R. R. Kerswell, *Nonlinearity* **18**, R17 (2005).
- [2] B. Eckhardt, T. M. Schneider, B. Hof, and J. Westerweel, *Annu. Rev. Fluid Mech.* **39**, 447 (2007).
- [3] G. Kawahara, M. Uhlmann, and L. van Veen, *Annu. Rev. Fluid Mech.* **44**, 203 (2012).
- [4] N. B. Budanur, K. Y. Short, M. Farazmand, A. P. Willis, and P. Cvitanović, *J. Fluid Mech.* **833**, 274 (2017).
- [5] B. Suri, L. Kageorge, R. O. Grigoriev, and M. F. Schatz, *Phys. Rev. Lett.* **125**, 064501 (2020).
- [6] G. Yalniz, B. Hof, and N. B. Budanur, *Phys. Rev. Lett.* **126**, 244502 (2021).
- [7] B. Hof, C. W. H. van Doorne, J. Westerweel, F. T. M. Nieuwstadt, H. Faisst, B. Eckhardt, H. Wedin, R. R. Kerswell, and F. Waleffe, *Science* **305**, 1594 (2004).
- [8] T. Kreilos and B. Eckhardt, *Chaos* **22**, 047505 (2012).
- [9] M. Avila, F. Mellibovsky, N. Roland, and B. Hof, *Phys. Rev. Lett.* **110**, 224502 (2013).
- [10] S. Zammert and B. Eckhardt, *Phys. Rev. E* **91**, 041003(R) (2015).
- [11] P. Ritter, F. Mellibovsky, and M. Avila, *New J. Phys.* **18**, 083031 (2016).
- [12] J. R. T. Lestro, G. Kawahara, L. van Veen, M. Shimizu, and H. Kokubu, *J. Fluid Mech.* **862**, R2 (2019).
- [13] C. Grebogi, E. Ott, and J. A. Yorke, *Phys. Rev. Lett.* **48**, 1507 (1982).
- [14] Y. Duguet, A. P. Willis, and R. R. Kerswell, *J. Fluid Mech.* **613**, 255 (2008).

- [15] D. P. Lathrop, J. Fineberg, and H. L. Swinney, *Phys. Rev. A* **46**, 6390 (1992).
- [16] M. Shimizu and P. Manneville, *Phys. Rev. Fluids* **4**, 113903 (2019).
- [17] C. S. Paranjape, Onset of turbulence in plane Poiseuille flow, Ph.D. thesis, Institute of Science and Technology Austria, 2019.
- [18] P. V. Kashyap, Y. Duguet, and O. Dauchot, *Entropy* **22**, 1001 (2020).
- [19] P. V. Kashyap, Y. Duguet, and O. Dauchot, *Phys. Rev. Lett.* **129**, 244501 (2022).
- [20] V. Mukund, C. S. Paranjape, M. P. Sitte, and B. Hof, arXiv:2112.06537.
- [21] L. S. Tuckerman, M. Chantry, and D. Barkley, *Annu. Rev. Fluid Mech.* **52**, 343 (2020).
- [22] L. S. Tuckerman, T. Kreilos, H. Schrobsdorff, T. M. Schneider, and J. F. Gibson, *Phys. Fluids* **26**, 114103 (2014).
- [23] A. P. Willis, *SoftwareX* **6**, 124 (2017).
- [24] X. Xiao and B. Song, *J. Fluid Mech.* **883**, R1 (2020).
- [25] J. F. Gibson, A spectral Navier-Stokes simulator in C++. Tech. Rep. (U. New Hampshire, 2012), www.channelflow.org.
- [26] J. Kim, P. Moin, and R. Moser, *J. Fluid Mech.* **177**, 133 (1987).
- [27] See Supplemental Material at <http://link.aps.org/supplemental/10.1103/PhysRevLett.131.034002> for (i) a movie illustrating the descent process, (ii) relation of the tilted to nontilted coordinate systems, (iii) further details on invariant solutions, (iv) bifurcation sequence in a larger domain, and (v) high Re simulations in tilted and nontilted domains.
- [28] Y. Duguet and P. Schlatter, *Phys. Rev. Lett.* **110**, 034502 (2013).
- [29] D. Viswanath, *J. Fluid Mech.* **580**, 339 (2007).
- [30] C. S. Paranjape, Y. Duguet, and B. Hof, *J. Fluid Mech.* **897**, A7 (2020).
- [31] H. E. Hurst, *Trans. Am. Soc. Civ. Eng.* **116**, 770 (1951).
- [32] B. B. Mandelbrot, *The Fractal Geometry of Nature* (W. H. Freeman and Co., San Francisco, 1982).
- [33] B. Hof, J. Westerweel, T. M. Schneider, and B. Eckhardt, *Nature (London)* **443**, 59 (2006).
- [34] B. Hof, A. de Lozar, D. J. Kuik, and J. Westerweel, *Phys. Rev. Lett.* **101**, 214501 (2008).
- [35] P. Grassberger and I. Procaccia, *Phys. Rev. Lett.* **50**, 346 (1983).
- [36] R. Hegger, H. Kantz, and T. Schreiber, *Chaos* **9**, 413 (1999).
- [37] J.-P. Eckmann and D. Ruelle, *Physica (Amsterdam)* **56D**, 185 (1992).
- [38] A. Brandstater and H. L. Swinney, *Phys. Rev. A* **35**, 2207 (1987).
- [39] L. Keefe, P. Moin, and J. Kim, *J. Fluid Mech.* **242**, 1 (1992).
- [40] K. Avila, D. Moxeu, A. de Lozar, M. Avila, D. Barkley, and B. Hof, *Science* **333**, 192 (2011).
- [41] L. Shi, M. Avila, and B. Hof, *Phys. Rev. Lett.* **110**, 204502 (2013).
- [42] S. Gomé, L. S. Tuckerman, and D. Barkley, *Phys. Rev. Fluids* **5**, 083905 (2020).
- [43] G. Lemoult, L. Shi, K. Avila, S. V. Jalikop, M. Avila, and B. Hof, *Nat. Phys.* **12**, 254 (2016).
- [44] M. Chantry, L. S. Tuckerman, and D. Barkley, *J. Fluid Mech.* **824**, R1 (2017).
- [45] L. Klotz, G. Lemoult, K. Avila, and B. Hof, *Phys. Rev. Lett.* **128**, 014502 (2022).
- [46] B. Hof, *Nat. Rev. Phys.* **5**, 62 (2023).
- [47] G. I. Taylor, *Phil. Trans. R. Soc. Lond.* **223**, 289 (1923).
- [48] S. Zammert and B. Eckhardt, *J. Fluid Mech.* **761**, 348 (2014).
- [49] T. Kanazawa, Lifetime and growing process of localized turbulence in plane channel flow, Ph.D. thesis, Osaka University, 2018.